Water retention in discrete element method

Yixiang Gan, Federico Maggi and Itai Einav

School of Civil Engineering, The University of Sydney, NSW 2006, Australia

Abstract. We describe water movement and retention using the discrete element method in view of future modelling of partially saturated granular materials. By defining the water potential in terms of capillary bridges at low saturation, and in terms of pressure of entrapped air at high saturation, we investigate the hysteresis of water retention in granular materials during wetting and drainage. These phenomena are successfully underpinned by our model thanks to an equation that determines the local evolution of liquid-solid contact angles at the level of pores and grains.

Keywords: water retention, discrete element method, partially saturated granular materials

INTRODUCTION

Water retention in partially saturated soil is fundamental in soil mechanics [1, 2, 3, 4], and has important implications in soil management and agriculture [5, 6, 7], and water purification [8, 9]. The collective behaviour of partially saturated soil depends on the structural network of the solids, liquids and gasses making this material, and the interfaces between them. The structural network is defined by the pore size distribution [10, 11], and the distributions of grain sizes and shapes [5, 6]; the interfaces between the phases are defined by the profile of the grain surfaces and the relative hydrophilicity of the grains and the fluids [12, 13, 14].

Existing phenomenological models [15, 16, 6, 17] usually need a set of fitting parameters that do not necessarily have a direct physical meaning. The connection between those models and grain-scale properties is usually unclear or qualitative, where the fitting is state dependent. For example, two sets of parameters are needed for the van Genuchten equation to reproduce retention curves during drainage and wetting.

With the aid of discrete element methods (DEM) [18], the numerical modelling of water flow in partially saturated media is feasible with even moderate computational capability. DEM with added inter-granular capillary interactions have been proposed by various authors [11, 19, 20, 21, 22], and the capillary forces between the grains usually deal with low saturation. For fully saturated granular materials, an extension of DEM incorporates computational fluid dynamics to include grain-liquid interaction [23]. However, a DEM model bridging pendular, funicular, and fully saturated states is still missing in literature.

The aim of this paper is to introduce a computational DEM framework for partially saturated granular materials, which is coupled with a newly-developed homogenisation scheme designed to connect local and averaged water potentials. The DEM framework is based on the description of local water movement between neighbouring cells, each containing a single grain. The homogenisation scheme is applied to determine water retention curves–that describe the averaged water potential against the averaged degree of saturation during hydraulic hysteresis cycles of wetting and drainage.

GRAIN-SCALE PROPERTIES

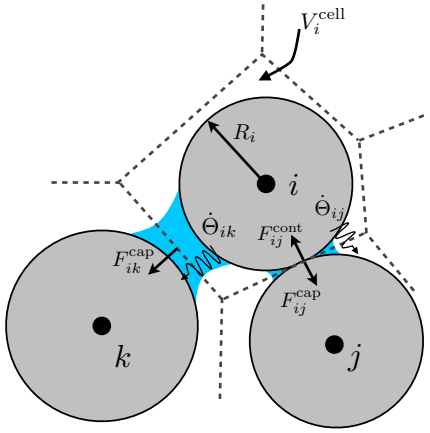

FIGURE 1. Schematics of three grains (grains' centres indicated by i, j and k) with connecting capillary bridges. The space has been divided using Voronoi tessellation, and water volumes within the cells vary by mass flux through cell boundaries, as $\dot{\Theta}_{ij}$ and $\dot{\Theta}_{ik}$.

Grain-scale properties are defined in relation to tessellated cells. Each cell in the computational domain is occupied by a single grain (Figure 1) by means of a modified Voronoi tessellation [24]. The total volume, V^{total}, is equal to the sum of Voronoi volumes V_i^{cell} centred around the corresponding grains. Each grain is associated with the cell's solid volume V_i^{solid}, water volume V_i^{water} and void volume $V_i^{\text{void}} = V_i^{\text{cell}} - V_i^{\text{solid}}$, with i

representing the i-th grain/cell. Global volumes are calculated using $V^{\text{void}} = \sum_i V_i^{\text{void}}$, $V^{\text{water}} = \sum_i V_i^{\text{water}}$ and $S_r = V^{\text{water}}/V^{\text{void}}$. The degree of saturation, void ratio and water content of the i-th grain/cell are defined by

$$S_{r,i} = \frac{V_i^{\text{water}}}{V_i^{\text{void}}} \, , \, \phi_i = \frac{V_i^{\text{void}}}{V_i^{\text{cell}}} \, , \, \Theta_i = \frac{V_i^{\text{water}}}{V_i^{\text{cell}}} \, . \tag{1}$$

Inter-granular forces are introduced to the DEM to represent the presence of water at the cell level. At the pendular regime, the capillary interaction between two grains is taken from an approximated solution to the governing Young-Laplace equation provided by Soulié et al. [25], in terms of the radii of grains i and j, (R_i and R_j), the gap distance and water volume of the capillary bridge between those grains, (V_{ij}^{br}), and the contact angle between water and grain (θ). We acknowledge that θ should evolve between receding and advancing angles (θ_{min} and θ_{max}, respectively). Here this evolution is assumed to take the following simple form

$$\dot{\theta} = \alpha \frac{\dot{V}_{ij}^{\text{br}}}{R_{\text{eff}}^3}, \quad \text{and } \theta_{\text{min}} \leq \theta \leq \theta_{\text{max}} \, , \tag{2}$$

where $\dot{V}^{\text{br}}$ is the rate of change of water volume of this capillary bridge, α is a non-dimensional coefficient, and R_{eff} is the effective radius $R_{\text{eff}} = 2R_iR_j/(R_i+R_j)$. The evolution of θ between θ_{min} and θ_{max} (see also Figure 2) is later shown to help us capturing hysteresis response during wetting and drainage.

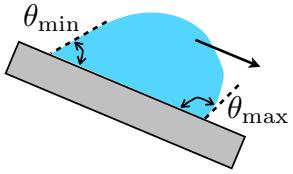

FIGURE 2. Contact angle limits, here shown for a water drop sliding along a tilted surface.

Beyond a local critical degree of saturation, S_r^0, when $S_r > S_r^0$, we move from the pendular regime to the funicular regime, where an increase of local water volume into the cell compresses the air volume. The local critical degree of saturation S_r^0 may depend on the grain's surface area through their fractal nature and it may be connected to the air entry value, but details will not be discussed here. We assume that the amount of gas substance, n, and its temperature, T are constant during wetting and drainage processes. According to the ideal gas law, $u^a V^a = nRT$, the relative air pressure can be calculated by

$$\Delta u^a = u^a - u_0^a = \begin{cases} 0 & \text{if } S_r \leq S_r^0 \\ \frac{S_r - S_r^0}{1 - S_r} u_0^a & \text{if } S_r > S_r^0 \end{cases} \, , \tag{3}$$

where u_0^a and u^a are the ambient and intrinsic air pressures, respectively.

HOMOGENISATION SCHEME

We develop a homogenisation scheme to determine collective water potential in terms of local quantities. According to a common definition in partially saturated soil mechanics, the effective stress (σ'_{ij}) is related to the net stress tensor $\sigma_{ij}^{\text{net}} = \sigma_{ij} - u_0^a \delta_{ij}$, water pressure ($u^w$) and air pressure ($u^a$) using [26]

$$\sigma_{ij}^{\text{net}} = \sigma'_{ij} - S_r \psi \delta_{ij} \, , \tag{4}$$

where $\psi = u_0^a - u^w$ is the water potential, and δ_{ij} is the Kronecker delta. Note that local air pressure is not the ambient air pressure u_0^a at the funicular regime.

Scholtes et al. [20] separates the total stress tensor into effective and capillary stress tensors,

$$\langle \sigma \rangle_{ij}^{\text{net}} = \langle \sigma \rangle'_{ij} + \langle \sigma \rangle_{ij}^{\text{cap}} = \frac{1}{V} \Big(\sum_c F_i^{\text{cont}} x_j + \sum_c F_i^{\text{cap}} x_j \Big) \, , \tag{5}$$

where $\mathbf{x}$ is the centre-to-centre distance between two neighbouring grains, with the contact and capillary forces defined by $\mathbf{F}^{\text{cont}}$ and $\mathbf{F}^{\text{cap}}$, respectively. The expression $\langle \cdot \rangle$ indicates a volume average. A more general equilibrium equation should introduce forces due to air pressure,

$$\begin{aligned} \langle \sigma \rangle_{ij}^{\text{net}} &= \langle \sigma \rangle'_{ij} + \langle \sigma \rangle_{ij}^{\text{cap}} + \langle \sigma \rangle_{ij}^{\text{air}} \\ &= \frac{1}{V} \Big(\sum_c F_i^{\text{cont}} x_j + \sum_c F_i^{\text{cap}} x_j + \sum_g \Delta u_g^a V_g^{\text{cell}} \delta_{ij} \Big) \, , \end{aligned} \tag{6}$$

where we correlate the effective stress tensor, $\langle \sigma \rangle'_{ij}$ to the inter-granular contact forces, $\mathbf{F}^{\text{cont}}$, the capillary stress tensor $\langle \sigma \rangle_{ij}^{\text{cap}}$ to the capillary forces $\mathbf{F}^{\text{cap}}$, and the intrinsic air pressure $\langle \sigma \rangle_{ij}^{\text{air}}$ to the local air pressure. Comparing Eq. (4) with Eq. (6), we find that

$$\langle \sigma \rangle_{ij}^{\text{cap}} + \langle \sigma \rangle_{ij}^{\text{air}} = -S_r \psi \delta_{ij} \, , \tag{7}$$

which gives the water potential ψ in terms of homogenised quantities,

$$\psi = -\frac{1}{3 S_r V} \Big(\sum_c F_i^{\text{cap}} x_i + \sum_g \Delta u_g^a V_g^{\text{cell}} \Big) \, , \tag{8}$$

where $\Delta u_g^a = u_g^a - u_0^a$ represents the local air pressure. The first term dominates at low saturations, while the second term dominates near saturation. These definitions in this homogenisation scheme may be extended to include systems with more than one component per phase [27].

For partially saturated soils water fluxes are defined by Richards equation [15]. Assuming gravity along the z-direction, and using $K(\Theta)$ as the hydraulic conductivity, the Richards equation becomes

$$\frac{\partial \Theta}{\partial t} = \nabla \Big[K(\Theta) \nabla (\psi + \rho g z) \Big] \,. \tag{9}$$

We can integrate Eq. (9) through the volume. According to the divergence theorem this can be calculated by the surface integration:

$$\int \frac{\partial \Theta}{\partial t} \mathrm{d}V = \oint \boldsymbol{\phi} \cdot \boldsymbol{n} \, \mathrm{d}S, \tag{10}$$

where, the water flux $\boldsymbol{\phi} = K(\Theta)\nabla(\psi + \rho g z)$, and $\boldsymbol{n}$ is the surface normal. In the DEM the water potential can be specified for grain i by ψ_i using a similar expression to Eq. (8) related only to the local cell/grain. The change of local water volume can be calculated using the individual fluxes between its neighbouring grains, through the discrete version of Eq. (10),

$$\begin{aligned} \mathrm{d}V_i^{\text{water}} &= \mathrm{d}(\Theta \cdot V_i^{\text{cell}}) = -\sum_j \phi_{ij}^{\text{water}} A_{ij} \mathrm{d}t \,, \\ \phi_{ij}^{\text{water}} &= -\frac{K_0}{|\mathbf{x}_j - \mathbf{x}_i|} \Big[\psi_j - \psi_i + \rho g (z_j - z_i) \Big] \,. \end{aligned} \tag{11}$$

We assume there is only a negligible change of cell volume during individual iterations, i.e., $\mathrm{d}V_i^{\text{cell}} \approx 0$. Note, we have replaced the hydraulic conductivity with a constant K_0 for the sake of simplicity, and A_{ij} is the effective conduction area, i.e., the cross-sectional area of the water along the Voronoi ij boundary.

RESULTS

We use a three-dimensional simulation domain consisting of 2,500 grains. The grains are nearly mono-sized with 5% variation in diameter. The mechanical boundary conditions are periodic for grain dynamics. An initial porosity ϕ =37% is being achieved by a stage of pre-compaction from a looser state. The hydraulic boundary conditions involve water inflow through a positive water pressure difference from the top while wetting, and a water outflow through a negative water pressure difference from the bottom during drainage (Figure 3). The wetting and drainage processes were applied to complete a survey cycle between predefined maximum and minimum saturations for the whole simulation domain. During the wetting and drainage cycles, the domain volume is fixed, i.e., constant porosity. The collective water potential, ψ, is calculated using Eq. (8).

We choose $\theta_{\min} = 5^\circ$ and $\theta_{\max} = 60^\circ$, as an example. There are three cases of cycles: S_r between 0.1 and 0.9, 0.2 and 0.8, and 0.4 and 0.6 (Figure 3). The envelope of the scanning curve is due to the overall behaviour of contact angles. In the transition between drainage and wetting, the local contact angle determines the actual overall dynamics of the potential. The dynamics of the contact angle embedded in Eq. (2) is the key behind our model ability to reproduce realistic hysteresis cycles during drainage and wetting. The shape of the hysteresis during transitions from drainage to wetting (and vice versa) is strongly influenced by this equation, as we observed strong sensitivity to the parameter α. The homogenised water potential increases during drainage, due to increase in F^{cap} and decrease in S_r, as reflected by Eq. (8).

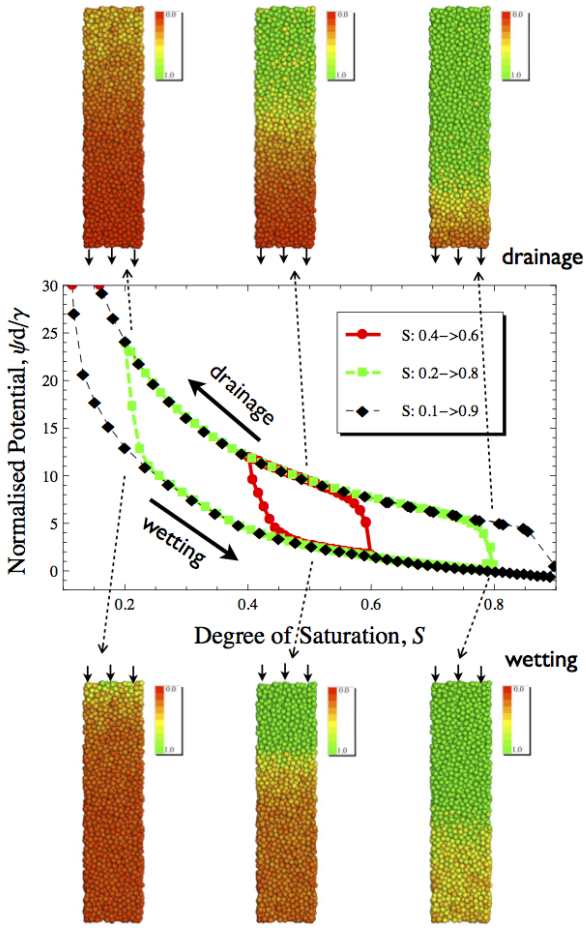

FIGURE 3. Water retention hysteresis using $\theta_{\min} = 5^\circ$ and $\theta_{\max} = 60^\circ$. Water potential ψ is normalised using grain size d and surface tension γ. The arrows show the directions of drainage and wetting processes, and six profiles show the local water distribution coloured by the degree of saturation with the scale between 0 and 1.

The proposed method is advantageous in offering insights into local grain-scale informations, such as distributions of local water contents and potential during

the wetting-drainage cycles. Figure 3 presents six temporal snapshots of spatial-distributed water content during both drainage and wetting between $0.1 \leq S_r \leq 0.9$. Future work will include sensitivity analyses to the effects of grain size, porosity and hydraulic conductivity.

CONCLUSIONS

We proposed a computational DEM framework to model the retention of fluids during wetting and drainage of partially saturated granular materials. By supporting this method with a new homogenisation scheme, and employing grain-level quantities of water content and potential, this study demonstrates how small scale hydromechanics control the phenomenology of larger scale water retention. Within the content of this study, a major factor affecting the hysteresis of water retention during cycles of wetting and drainage came from the way we described the dynamics of the solid-liquid contact angles as a function of the change of the local water volumes.

ACKNOWLEDGMENTS

Financial support for this research from the Australian Research Council through Grant No. DP120104926 and DE130101639 is gratefully appreciated.

REFERENCES

1. B. Loret, and N. Khalili, *Mechanics of Materials* **34**, 97–116 (2002).
2. M. Nuth, and L. Laloui, *Computers and Geotechnics* **35**, 835–844 (2008).
3. D. Sheng, a. Gens, D. Fredlund, and S. Sloan, *Computers and Geotechnics* **35**, 810–824 (2008).
4. G. Buscarnera, and I. Einav, *Géotechnique* **62**, 147–160 (2012).
5. J. M. Blonquist, S. B. Jones, I. Lebron, and D. a. Robinson, *Water Resources Research* **42**, 1–13 (2006).
6. R. Heinse, S. B. Jones, S. L. Steinberg, M. Tuller, and D. Or, *Vadose Zone Journal* **6**, 713 (2007).
7. C. Gu, F. Maggi, W. J. Riley, G. M. Hornberger, T. Xu, C. M. Oldenburg, N. Spycher, N. L. Miller, R. T. Venterea, and C. Steefel, *Journal of Geophysical Research* **114**, G01006 (2009).
8. L. C. Schideman, B. J. Mariñas, V. L. Snoeyink, and C. Campos, *Environmental science & technology* **40**, 6805–11 (2006).
9. M. L. Magnuson, and T. F. Speth, *Environmental science & technology* **39**, 7706–11 (2005).
10. a. Revil, and L. M. Cathles, *Water Resources Research* **35**, 651 (1999).
11. J. a. Gili, and E. E. Alonso, *International Journal for Numerical and Analytical Methods in Geomechanics* **26**, 433–468 (2002).
12. M. Goebel, J. Bachmann, S. Woche, W. Fisher, and R. Horton, *Soil Science Society of* ... pp. 383–393 (2004).
13. J. Bachmann, S. Woche, M. Goebel, M. Kirkham, and R. Horton, *Water Resources Research* **39**, 1353 (2003).
14. A. Russell, and O. Buzzi, *Geotechnique* **62**, 269 –274 (2012).
15. L. Richards, *Physics* **1**, 318 (1931).
16. M. van Genuchten, *Soil Science Society of America Journal* **44**, 892–898 (1980).
17. F. Maggi, and C. Pallud, *Planetary and Space Science* **58**, 1996–2007 (2010).
18. P. A. Cundall, and O. D. L. Strack, *Géotechnique* **29**, 47–65 (1979).
19. M. Jiang, S. Leroueil, and J. Konrad, *Computers and Geotechnics* **31**, 473–489 (2004).
20. L. Scholtes, P. Hicher, F. Nicot, B. Chareyre, and F. Darve, *International Journal for Numerical and Analytical Methods in Geomechanics* **33**, 1289–1313 (2009).
21. J.-P. Gras, J.-Y. Delenne, F. Soulié, and M. El Youssoufi, *Powder Technology* **208**, 296–300 (2011).
22. B. Chareyre, A. Cortis, and C. E. Barth, *Transport in Porous Media* **94**, 595–615 (2012).
23. A. Di Renzo, and F. P. Di Maio, *Chemical Engineering Science* **62**, 116–130 (2007).
24. C. Rycroft, G. Grest, J. Landry, and M. Bazant, *Physical Review E* **74**, 021306 (2006).
25. F. Soulié, F. Cherblanc, M. El Youssoufi, and C. Saix, *International Journal for Numerical and Analytical Methods in Geomechanics* **30**, 213–228 (2006).
26. G. T. Houlsby, *Geotechnique* **47**, 193–196 (1997).
27. F. Maggi, *Colloids and Surfaces A: Physicochemical and Engineering Aspects* **415**, 119–124 (2012).